frontiers | Frontiers in Marine Science

TYPE Original Research
PUBLISHED 08 September 2022
DOI 10.3389/fmars.2022.1005663

OPEN ACCESS

EDITED BY
Zhiyong Lin,
University of Hamburg, Germany

REVIEWED BY
Dong Feng,
Shanghai Ocean University, China
Jiarui Liu,
University of California, Los Angeles, United States

*CORRESPONDENCE
Xiting Liu
liuxiting@ouc.edu.cn
Jing Chen
jchen@geo.ecnu.edu.cn

SPECIALTY SECTION
This article was submitted to Marine Biogeochemistry, a section of the journal Frontiers in Marine Science

RECEIVED 28 July 2022
ACCEPTED 22 August 2022
PUBLISHED 08 September 2022

CITATION
Chang X, Liu X, Wang H, Zhuang G, Ma Z, Yu J and Chen J (2022) Depositional control on the sulfur content and isotope of sedimentary pyrite from the southeast coast of China since MIS5. *Front. Mar. Sci.* 9:1005663. doi: 10.3389/fmars.2022.1005663

Depositional control on the sulfur content and isotope of sedimentary pyrite from the southeast coast of China since MIS5

Xin Chang[1], Xiting Liu[1,2]*, Houjie Wang[1,2], Guangchao Zhuang[3], Zhixin Ma[4], Junjie Yu[5] and Jing Chen[6]*

[1]Key Laboratory of Submarine Geosciences and Prospecting Technology, College of Marine Geosciences, Ocean University of China, Qingdao, China, [2]Laboratory for Marine Geology, Qingdao National Laboratory for Marine Science and Technology, Qingdao, China, [3]Frontiers Science Center for Deep Ocean Multispheres and Earth System (FDOMES) and Key Laboratory of Marine Chemistry Theory and Technology, Ministry of Education, Ocean University of China, Qingdao, China, [4]School of Ocean Sciences, China University of Geosciences, Beijing, China, [5]Nanjing Center, China Geological Survey, Nanjing, China, [6]State Key Laboratory of Estuarine and Coastal Research, East China Normal University, Shanghai, China

The content and isotopic composition of pyrite sulfur are significantly affected by local depositional conditions and are sensitive to environmental evolution. Here, we use core QK11, collected from Xiapu Bay, southeast coast of China, to reveal how local depositional conditions constrained pyrite formation and sulfur isotopic composition since MIS5. Our results show that the content of pyrite sulfur is mainly controlled by the TOC content during interglacial intervals and is limited by the supplement of sulfate in glacial intervals. Therefore, the C/S ratios can effectively identify three transgressions since MIS5. The sulfur isotopic composition of pyrite ranges from -36.7 to 18.4‰ in the whole core. The occurrence of isotopically "heavy" pyrite is observed at the depth of 2.2~9.2, 27.2~33.8, and 43.5~62.5 mbsf, which is attributed to the influence of sulfate reservoir effect, depositional event, unsteady diagenetic environment, and other factors, highlighting the influence of local depositional and diagenetic processes on the isotopic composition of pyrite sulfur. Pyrite sulfur in other layers is generally depleted in ^{34}S, as low as -36.7‰, indicating that the early-stage organiclastic sulfate reduction (OSR) plays an important role in sulfur isotopic fractionation. The results also suggest that organic carbon indicators (TOC/TN ratio and $\delta^{13}C$) combined with the C/S ratio can effectively distinguish between freshwater and marine environments, which is of great significance to reveal depositional evolution in deep time.

KEYWORDS

pyrite, sulfur isotope, organic carbon, sedimentary environment, East China Sea

Introduction

Pyrite (FeS_2) represents the main sulfur sink of marine sediments, which has been widely employed to trace the global sulfur cycle, biological evolution, and redox conditions in Earth's surface environment (Berner, 1984; Raiswell and Canfield, 2012; Fike et al., 2015; Fakhraee et al., 2019). In the sediments deposited on the continental margins, the sulfide used to form pyrite is mainly derived from sulfate reduction. During the sulfate reduction process, microbes preferentially utilize the isotopically lighter sulfur in sulfate to produce sulfides, so the produced pyrite is depleted in ^{34}S relative to the initial sulfate, resulting in a large sulfur isotopic fractionation (Jørgensen, 1982; Habicht and Canfield, 1997). In spite of the control of microbial metabolism, recent studies have suggested that the sulfur isotopic composition of pyrite ($\delta^{34}S_{py}$) is also affected by local depositional factors (Lang et al., 2020; Houghton et al., 2021; Liu et al., 2021a), which could be preserved in the sedimentary record. For example, recent studies showed that the high sedimentation rates are conducive to the formation of the relative "closed" diagenetic system, leading to the formation of isotopically "heavy" pyrite (Pasquier et al., 2017; Liu et al., 2019).

Other processes that may cause the enrichment of ^{34}S in pyrite are as follows. In a system with low-sulfate concentration, when the sulfate is completely consumed by the sulfate reduction process, the produced sulfide will inherit the sulfur isotopic composition of the original sulfate pool with a minor isotopic fractionation (Gomes and Hurtgen, 2013). As sediments are buried deeper, the communication between porewater and overlying seawater is limited, resulting in a simultaneous increase in sulfur isotope of porewater sulfate and produced sulfides in a "closed" diagenetic system (Canfield, 2001; Liu et al., 2020a). In methane-rich environments, anaerobic methane oxidation (AOM) can be coupled with sulfate reduction, leading to pyrite formation with high content and heavy sulfur isotope in the sulfate-methane transition zone (Jørgensen et al., 2004; Borowski et al., 2013; Lin et al., 2017). The diffusion of hydrogen sulfide (H_2S) driven by porewater sulfide concentration gradient would result in large differences in diagenetic processes and isotopic composition of pyrite sulfur between different layers (Liu et al., 2021b). Abiotic oxidation of sulfide to sulfate, due to frequent, repeated oxidative reworking in the shallow marine environment, would modulate the $\delta^{34}S$ signals in sedimentary pyrite (Fry et al., 1988; Aller et al., 2010). However, the relationship between local depositional conditions and sulfur isotopic composition is complex, and the specific constraint mechanism between them requires further research.

The East China Sea (ECS) receives a lot of terrestrial sediment and organic matter from the Changjiang River and many other local rivers from Zhejiang, Fujiang, and Taiwan (Liu et al., 2018a). Under the influence of wave, tide, and current, several mud depocenters with high contents of organic carbon and fine-grain sediments were developed, which provide a natural laboratory to study how depositional processes control pyrite formation and its geochemical composition (Liu et al., 2018a; Zhao et al., 2018; Zhang et al., 2021). In this study, we analyzed the core QK11, collected from the southeast coast of China, to reveal how the depositional evolution constrains the pyrite formation and its sulfur isotope since MIS5.

Regional setting

The ECS is one of the typical river-dominated marginal oceans, which receives a large amount of terrestrial material input from the Changjiang River as well as numerous mountainous rivers, including Oujiang, Minjiang, and Zhuoshuixi (Figure 1A). The current system in the ECS inner shelf modulates the transport and deposition of terrestrial

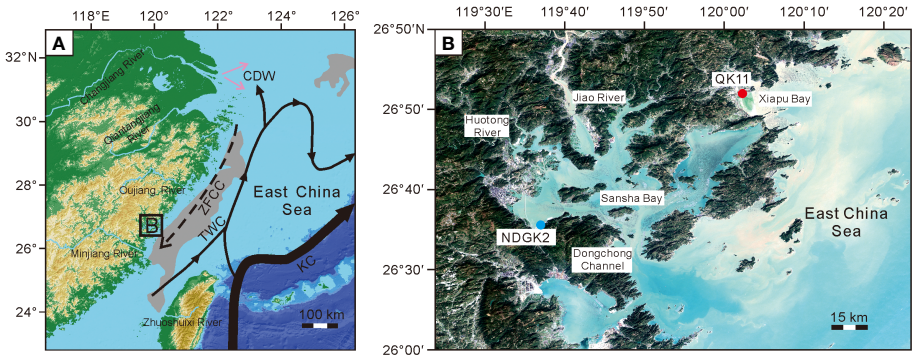

FIGURE 1
Regional setting and core location of core QK11. **(A)** The distribution of mud sediments on the East China Sea inner shelf with the current system (Liu et al., 2006). KC, Kuroshio Current; TWC, Taiwan Warm Current; ZFCC, Zhejiang-Fujian Coastal Current. **(B)** Xiapu Bay, the locations of core QK11 (Red dot, this study) and core NDGK2 (blue dot, Dai et al., 2021).

sediment (Zhang et al., 2019), including the Changjiang diluted water (CDW), Zhejiang-Fujian coastal current (ZFCC), and Taiwan warm current (TWC) (Figure 1A). And a mud depocenter was formed under such sedimentary conditions, which is distributed in a northeast-southwest direction along the coast of Zhejiang and Fujian (Liu et al., 2006; Liu et al., 2007; Dong et al., 2018; Dong et al., 2020; Dong et al., 2021). Xiapu Bay, the study area, is located in the northern Fujian Province along the ECS (Figure 1B). Luohanxi and Beixi Rivers are the two main rivers that flow into Xiapu Bay, but the runoff sediment flux can be almost neglected compared to sediments from the inner shelf of the ECS transported by tidal currents (Sun et al., 2022).

A series of core data from the Bohai Sea, Yellow Sea, East China Sea, and South China Sea demonstrated that the Chinese marginal seas have experienced three transgressions, corresponding to MIS5, MIS3, and MIS1, respectively (Waelbroeck et al., 2002; Lisiecki and Raymo, 2005; Wang et al., 2020). However, on the ECS coast, especially the coast area of Zhejiang and Fujian, only one or two transgressive strata were developed, and the period and magnitude of marine transgression are still a controversial topic (Geng, 1982; Zhao et al., 2008; Lin and Dai, 2012). In recent studies of cores collected from Sansha Bay and Xiapu Bay, three transgressive events since MIS5 were identified using geochemical indicators, palynology, and micropalaeontology, which established a well stratigraphic and sedimentologic framework for our study (Dai et al., 2021; Yu et al., 2021; Sun et al., 2022; Wang et al., 2022).

Materials and methods

Core QK11

The core QK11 is located in Xiapu Bay, northern Fujian Province (26.88°N, 120.05°E, Figure 1B), with a length of 70.6 m and an orifice elevation of 6 m. There is a homogeneous layer filled with clay at the depth of 70.6~69.8 mbsf (Figure 2). The sediments deposited at the depth of 69.8~37.7 mbsf are generally coarse-grained, consisting mainly of pebble-bearing sand or sand-bearing pebble layers, interspersed with several thin intervals of clay and sand. The strata at the depth of 37.7-20.8 mbsf is a set of homogeneous clay layers with shell fragments, and the sediment is dramatically coarsened at about 34-31 mbsf. At the depth of 20.8~16.1 mbsf, the sediments are composed of mainly hard clay. The deposits above 16.1 mbsf are muddy clay layers with a large amount of shell and carbonized plant fragments.

Pyrite sulfur analysis

Pyrite sulfur in bulk sediments was obtained by the method described by Canfield et al. (1986). Under constant flow of nitrogen or argon gas, the sediments were heated to 186°C (± 10°C) in a solution of 6 M HCl and 2 M chromium (II) chloride and stirred for 4 h. Reduced sulfur in sediments was released as hydrogen sulfide and captured as precipitation of silver sulfide in a test tube containing silver nitrate solution. After rinsing, drying, and weighing, the contents of chromium-reducible sulfur (CRS) in bulk sediment were calculated gravimetrically. In this paper, we analyzed CRS content as pyrite sulfur content.

Gas chromatography-isotope ratio mass spectrometry (GC-IRMS) was used to analyze the sulfur isotopic composition in CRS. The Instrument model: Delta V Plus GC-IRMS (Thermo Fisher Science), Sensitivity is better than 1200 M/I, error < 0.1‰; Detection error: RMs (IAEAS1, IAEAS2, IAEAS3) standard deviation < 0.3‰, analysis error < 0.1‰.

Total organic carbon and total nitrogen analysis

The contents and isotope analysis of TOC and TN were carried out in the Key Lab of Submarine Geosciences and Prospecting Techniques, MOE, China. The test instruments are an EA-IsoLink elemental analyzer with a MAS 200R autosampler coupled to a MAT253 plus isotope ratio mass spectrometer *via* a ConFlo IV universal interface (all from Thermo Fisher Scientific, Bremen, Germany). The Elemental Technology Co. Ltd. reference material, IVA33802180, is a soil standard sample with a total carbon content of 0.83 ± 0.05% and 0.07 ± 0.01% nitrogen, used as a routine working standard for the content determination of carbon and nitrogen. The contents of TOC and TN were calculated by standard curves and the accuracy can be estimated to be around 3% RSD. The international reference materials (RMs): USGS40 (L-glutamic), USGS64 (glycine), and USGS24 (graphite) (all from NIST, US), were used in this study. The $\delta^{13}C$ values certified by USGS40, USGS64, and USGS24 as the mean ± 95% confidence is -26.39 ± 0.09‰, -40.81 ± 0.04‰, and -16.05 ± 0.04‰, respectively. The precision for $\delta^{13}C$ is ± 0.06‰ (1σ) for 30 μg of carbon.

Results

Chronology and pyrite of core QK11

The chronology of core QK11 is referred to a well-established stratigraphic framework of core NDGK2 (Figure 2A), including ages from AMS^{14}C and optically stimulated luminescence (OSL), and relative stratigraphic correlation between them (Dai et al., 2021; Sun et al., 2022). According to previous work on core QK11 (Sun et al., 2022), the relative pyrite content in heavy minerals in core QK11 increases significantly during the interglacial stages, which corresponds to the intervals with high salinity reflected by increased Sr/Ba ratios (Figure 2B). Pyrite aggregates, main

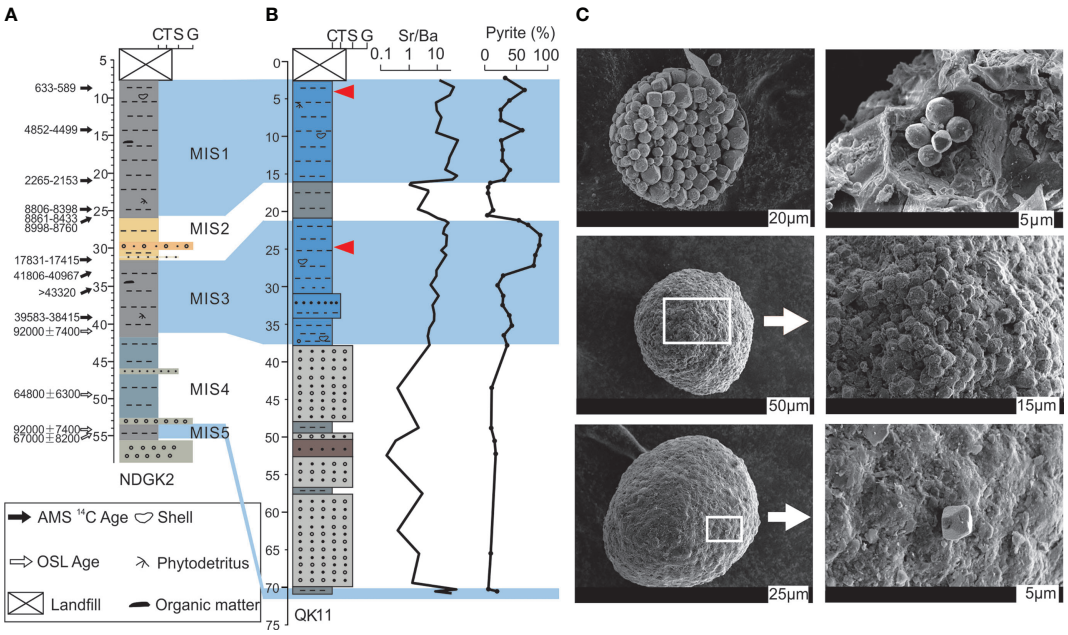

FIGURE 2
Chronology and pyrite of core QK11. **(A)** Dating of core NDGK2. **(B)** Sr/Ba ratio and relative content of pyrite in heavy minerals of core QK11. **(C)** Scanning electron microscope (SEM) photographs of pyrite aggregates. Age data are referred to Dai et al. (2021); the relative pyrite content in coarse (500~32 μm) heavy minerals are from Sun et al. (2022); The shaded regions indicate intervals of elevated relative contents of pyrite and increased Sr/Ba ratios during the interglacial MIS5, 3, and 1; The red arrows represent the sampling locations of pyrite photographs; The white rectangles represent the areas shown on the right in Figure 2C.

framboids with a large diameter (> 50 μm), consist of octahedral and irregular pyrite microcrystals (Figure 2C). According to the relative pyrite contents and previous research results (Dai et al., 2021; Sun et al., 2022), core QK11 is divided into five sedimentary intervals (Figure 2). Three interglacial intervals at depths of 70.6~70.2, 37.5~22.8, and 15.8~2.2 mbsf correspond to MIS5, MIS3, and MIS1, respectively, whereas glacial intervals at depth of 70.2~37.5 mbsf and 22.8~15.8 mbsf correspond to MIS4 and MIS2, respectively.

Pyrite sulfur content, isotopic composition, and C/S ratio

The CRS contents, representing the pyrite sulfur in the study area (Liu et al., 2020b), show a strong fluctuation coinciding with the glacial-interglacial cycles (Figure 3A). The contents of CRS are generally less than 1.13%, and maintain high values in clay layers. The coarse-grained sediments composed of silt and pebbles present low contents of CRS, most of which are below the detection limit (0.01%). We set the CRS values below the detection limit to 0.01% for the calculation of C/S ratios.

The $\delta^{34}S_{py}$ in core QK11 ranges from -36.7‰ to 18.4‰, with $\Delta^{34}S$ ($\delta^{34}S_{sulphate}$-$\delta^{34}S_{py}$) as high as 57.94‰, calculated from the sulfur isotopic composition of modern seawater sulfate (21‰, Tostevin et al., 2014). And the isotopically "heavy" pyrite occurs at the depth of 7.8~2.2, 33.8~27.2, and 43.5~62.5 mbsf (Figure 3B). The C/S ratio of core QK11 ranges from 0.91~38.46 and effectively divides glacial and interglacial sedimentary intervals (Figure 3C). C/S ratios of glacial intervals are high, with an average of 12.44, whereas the interglacial C/S ratios are generally less than 2.8. The average value of C/S ratios is only 1.47 in the lower part of the MIS1 interval, which increases significantly in the upper part accompanied by the decrease in CRS contents.

TOC and TN contents, $\delta^{13}C$ of TOC, and TOC/TN ratios

The contents of TOC and TN show no obvious trends in core QK11 (Figures 3D, E). TOC content ranges from 0.02 to 1.65% with an average of 0.47%. And the maximum value occurs at the depth of 33.8 mbsf. The TN contents of several samples in the lower half of the core are too low to obtain data, which were set as 0.01% and represented as a hollow circle in Figures 3E, G. There are no trends for TOC/TN ratio and $\delta^{13}C$ in the same way, but they all peak at the depth of 33.8 mbsf: TOC/TN ratio

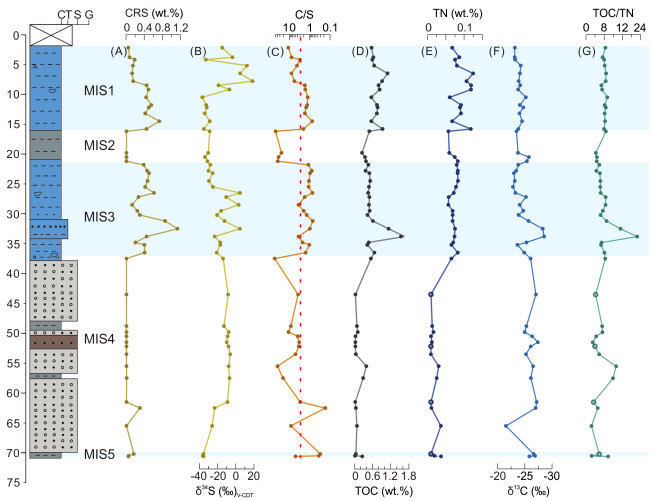

FIGURE 3
The lithology and contents of carbon, nitrogen, and sulfur abundance of core QK11. **(A, B)** The abundance of chromium-reducible sulfur (CRS) and the sulfur isotopic composition of CRS; **(C)** The ratio between total organic carbon and chromium-reducible sulfur (C/S); **(D-F)** The contents of total organic carbon (TOC) and total nitrogen (TN) and the isotopic composition of TOC; **(G)** The ratio between total organic carbon and total nitrogen (TOC/TN).

increases to 22.43, whereas $\delta^{13}C$ decreases to -28.53‰ (Figures 3F, G).

Discussion

Limiting factor for the formation of sedimentary pyrite

In organic mineralization, organic carbon is consumed as an electron donor in the sulfate reduction process, with the production of hydrogen sulfide (Fike et al., 2015). Although most of the products are reoxidized to sulfate, the remaining fraction of them are able to form metastable iron sulfide with the participation of reactive iron, and ultimately convert to sedimentary pyrite which is buried as the major sulfur sink in marginal sea sediments (Jørgensen, 1982; Berner, 1984; Rickard, 2012; Fike et al., 2015). The formation of sedimentary pyrite is greatly affected by the sedimentary conditions, including the quantity and reactivity of organic carbon, the availability of reactive iron, and the supplement of sulfate (Berner, 1984). Here, we analyze the above factors to demonstrate the main factor that impacts the formation of sedimentary pyrite in the study area since MIS5.

Pyrite is sensitive to reactive iron availability which has an important influence on the early diagenetic process of sediments (Shawar et al., 2018). In the Baltic and Black Seas, for example, with high organic carbon content but limited reactive iron supply in sediments, the residual porewater hydrogen sulfide diffuses downward from the marine mud to the underlying lacustrine clay and reacts with the reactive iron to form the sulfidization front (Jørgensen et al., 2004; Holmkvist et al., 2014; Liu et al., 2020a). However, the inner shelf of the ECS receives a large amount of terrestrial supply from large and medium-sized rivers such as the Yangtze River and Qiantang River, with an adequate supply of reactive iron (Huang and Lin, 1995; Lin et al., 2002; Wei et al., 2021). The availability of reactive iron does not limit the formation of sedimentary pyrite in the study area, although strong iron reduction may inhibit the sulfate reduction process (Kao et al., 2004).

Previous studies demonstrated a significant positive correlation between the organic burial rate and sulfate reduction rate, indicating that the sedimentary pyrite formation in the ECS shelf is mainly controlled by the organic carbon content (Lin et al., 2002). This perspective is also well verified in our results by a positive correlation between CRS and TOC contents in core QK11 (R^2 = 0.623) (Figure 4A), and the maximum of organic carbon contents corresponds to the peak of CRS contents (Figure 3). However, it should be noted that the contents of CRS are generally below the detection limit in glacial intervals, whereas the TOC varies between 0.1 and 0.4%, with an extremely low correlation coefficient (Figure 4A). Thus, the formation of sedimentary pyrite in glacial intervals should be affected by other factors besides the organic carbon contents

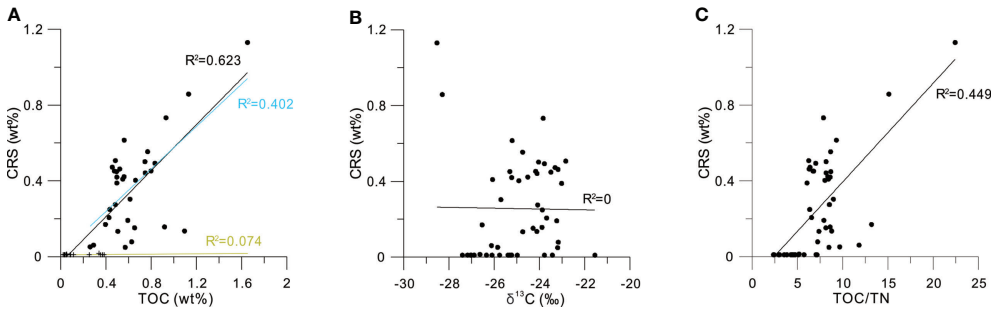

FIGURE 4
Sedimentary factors controlling CRS content in core QK11. **(A-C)** TOC content, $\delta^{13}C$ of TOC, and TOC/TN ratio *vs.* CRS content. The fit line of carbon and sulfur correlation of all samples in **(A)** is black, the blue line is for interglacial sediments (marine environment), and the yellow line is for the glacial sediments (freshwater environment).

(e.g., undersupply of porewater sulfate in the terrestrial environment). In the glacial intervals (MIS4 and 2), the freshwater environment caused by the low sea level could not provide enough sulfate to produce sulfide, which will finally suppress the formation of pyrite. When the study area was flooded during transgressive intervals (MIS5, 3, and 1), a decent sulfate supply would alleviate the limiting effect of sulfate on sulfide production. Therefore, the formation of sedimentary pyrite was dominated by the supplement of sulfate in the glacial intervals and mainly controlled by TOC content during interglacial intervals.

Previous studies suggested that the less reactive organic compounds would result in lower rates of sulfate reduction (Berner, 1984; Westrich and Berner, 1984). Thus, the source of organic carbon may potentially affect the formation of pyrite, because of the differences in reactivity between marine and terrestrial organic carbon (the latter is more refractory) (Blair and Aller, 2012). The TOC/TN ratio and $\delta^{13}C$ of organic carbon have been widely used as classical indicators to trace the source of organic carbon in sediments deposited on global estuaries and continental shelves dominated by large rivers (Bianchi et al., 2002; Zhan et al., 2011). We attempt to assess the possible influence of variation in reactivity of organic carbon on sedimentary pyrite during transgressive cycles by using them. No positive obvious correlation is observed between $\delta^{13}C$ and CRS content (Figure 4B). And the correlation between TOC/TN ratio and CRS is moderate, with an R^2 of 0.449 (Figure 4C). Due to the influence of possible "extra nitrogen source" (e.g., adsorption of inorganic nitrogen by clay minerals), the measured values of TOC/TN ratios in terrestrial sediments are significantly different from the actual values (Meyers, 1994; Meyers, 1997; Sampei et al., 1997; Sampei and Matsumoto, 2001; Hu et al., 2014). The average values of TOC/TN ratios in the two freshwater sedimentary intervals (MIS2 and MIS4) are 4.6 and 4.4, respectively, indicating a marine origin of organic carbon. Therefore, the correlation between CRS and TOC/TN ratio in core QK11 may not truly reflect their relationships, which needs careful evaluation.

Depositional evolution since MIS5 constrained by C/S ratios

Pyrite is usually more abundant in marine sediments than in fluvial and lacustrine sediments due to the differences in supplement of sulfate between them. The statistical results show that the C/S = 2.8 ± 1.5 can be used to distinguish the marine from the freshwater sedimentary environment (Berner and Raiswell, 1984; Raiswell and Canfield, 2012; Wei and Algeo, 2020). However, C/S ratios represent high values in certain marine environments as in the freshwater environment, such as the euxinic bottom water limited by iron, organic-rich environment promoted by upwelling, and unsteady diagenetic environment (Morse and Emeis, 1990; Lyons and Berner, 1992; Aller and Blair, 1996). Thus, when applying the C/S ratio to reveal the sedimentary history, it is necessary to combine other indicators (e.g., Sr/Ba ratio) (Liu et al., 2022). Based on previous studies, we evaluate the applicability of the C/S ratio to indicate depositional evolution in the Xiapu Bay since MIS5.

The C/S ratios of glacial sedimentary intervals in core QK11 are significantly higher than 2.8 (Figure 5), indicating a typical freshwater sedimentary environment (Berner and Raiswell, 1984). But some samples of the MIS4 interval have relatively low C/S ratios, even less than 2.8. This is mainly because the contents of CRS in this interval are extremely low, and most of them are below the detection limit (0.01%), thus the actual C/S ratios should be higher than the calculated values. Sedimentary conditions during glacial intervals, such as strong weathering, undersupply of porewater sulfate, and coarse-grained sediments with less TOC, would lead to poor formation and preservation of authigenic pyrite, followed by high C/S ratios.

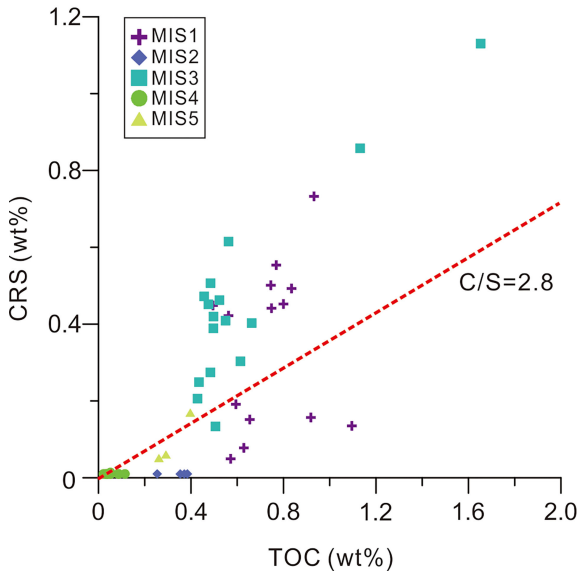

FIGURE 5
The correlation between the content of total organic carbon (TOC) and CRS (representing pyrite sulfur).

The C/S ratio in MIS5 ranges from 2.3 to 5.1, with an average of 4.1, and no foraminifera is observed in this interval (Sun et al., 2022). These sedimentary records seem to support that the sediments were deposited in a fluvial or lacustrine environment. However, this view needs to be questioned. In fact, C/S ratios cannot well distinguish the brackish environment from the marine environment because their ranges overlap considerably (Wei and Algeo, 2020). Compared with intervals of MIS4 and MIS2 with high C/S ratios, the C/S ratios of MIS5 interval are near the boundary values. The Sr/Ba ratio in this interval increases significantly (Figure 2B), which represents a depositional environment with increased salinity (Sun et al., 2022). In addition, the marine dinocyst record of NDGK2, located in Sansha Bay (Figure 1B), also suggests that the study area has experienced a marine incursion during MIS5 (Dai et al., 2021). We suggest that Xiapu Bay is influenced by seawater sulfate during MIS5, but the magnitude of transgression is weak so that the sedimentary environment is not conducive to the growth or later preservation of foraminifera.

The MIS1 interval is segmented in geochemical characteristics. The lower part is similar to the MIS3 interval. The evidence, including abundant pyrite aggregates, low C/S ratios, and foraminifera records, indicates a typical marine environment during this period (Sun et al., 2022). However, the upper part of MIS1 sediments is characterized by high C/S ratios and low CRS contents (Figure 3C). This phenomenon is attributed to the unsteady diagenetic environment along the ECS coast, which is consistent with previous results off the Zhejiang coast (Liu et al., 2018b; Liu et al., 2021c; Liu et al., 2022). In the unsteady diagenetic environment, the sulfate reduction is suppressed by iron reduction, and sulfides are oxidized to sulfate under strong hydrodynamic conditions and bioturbation, resulting in low CRS contents and high C/S ratios in surface sediments deposited on the ECS inner shelf (Ge et al., 2015; Zhu et al., 2016; Liu et al., 2018b).

C/S ratios show that the transgression in MIS5 is weak, whereas the transgressive events in MIS3 and MIS1 have a wider impact. Due to the unsteady diagenetic environment along the ECS coast, the sedimentary strata deposited in MIS1 is segmented in C/S ratio and CRS content. These findings demonstrate that the C/S ratio can effectively reveal the depositional evolution of Xiapu Bay since MIS5, and also emphasizes the necessity of combining different indicators in the reconstruction of the paleoenvironment (Liu et al., 2022).

Response of isotopic composition of pyrite sulfur to depositional evolution

The formation of pyrite in marine sediments plays a fundamental role in the biogeochemical carbon-sulfur-iron cycling and modulated the redox conditions on Earth's surface over geological timescales (Algeo et al., 2015). And the evolution history of Earth's surface environment was recorded in $\delta^{34}S_{py}$ extensively (Fike et al., 2015). Recent studies have demonstrated that $\delta^{34}S_{py}$ is significantly impacted by local depositional conditions in short timescales, suggesting that the isotopic

composition of pyrite sulfur is very sensitive to local depositional evolution rather than the global sulfur cycle (Pasquier et al., 2017; Liu et al., 2019; Liu et al., 2020b). Here, we carry out a series of geochemical analysis work of core QK11 to study the influence of depositional evolution on $\delta^{34}S_{py}$ during glacial-interglacial cycles since MIS5. On the whole, there is no obvious correlation between the $\delta^{34}S_{py}$ values and other geochemical parameters (TOC, $\delta^{13}C$, C/S ratio, TOC/TN ratio) in core QK11 (Figures 6A–D). It probably suggests that the sulfur isotopic composition of pyrite is influenced by multiple factors rather than a certain one. Since MIS5, the study area has experienced three transgressive events, and the discrepancy of local depositional conditions such as transgressive magnitude, organic carbon input, and sedimentation rate during these periods may have varying controls on the $\delta^{34}S_{py}$.

Previous studies have shown that bacterial sulfate reduction is associated with a strong isotopic fractionation, with sulfide and pyrite depleted in ^{34}S, and possibly reaching up to 70‰ (Sim et al., 2011). The $\delta^{34}S_{py}$ in sediments of Xiapu Bay deposited in MIS5 is stably negative and ranges from -35 to -40‰ generally with an offset of about 57‰. The considerable isotopic offset indicates that early-stage organiclastic sulfate reduction (OSR) plays an important role in pyrite formation, although the contribution of disproportionation in sulfur isotopic fractionation cannot be ruled out (Canfield and Thamdrup, 1994). Despite transgression being weak during MIS5, the supplement of sulfate is enough to protect $\delta^{34}S_{py}$ from the sulfate reservoir effect (Gomes and Hurtgen, 2013).

Xiapu Bay presented a typical marine environment during MIS3 revealed by C/S ratios, Sr/Ba ratios, and foraminifera records (Sun et al., 2022). But at the depth of 27~34 mbsf, lithologic and geochemical characteristics change significantly, with isotopically "heavy" pyrite in sediments correspondingly (Figure 3). The sediment type changed from clay and silt to coarser sand and gravel. TOC increased from 0.5% to 1.6%, resulting in the CRS peak in the whole core. The dramatic change of TOC/TN ratio and $\delta^{13}C$ at the depth of 32.5~33.8 mbsf indicates an important shift in the source of organic carbon, suggesting an increased input of terrestrial materials. Although not obvious, the phenomenon of source shift of

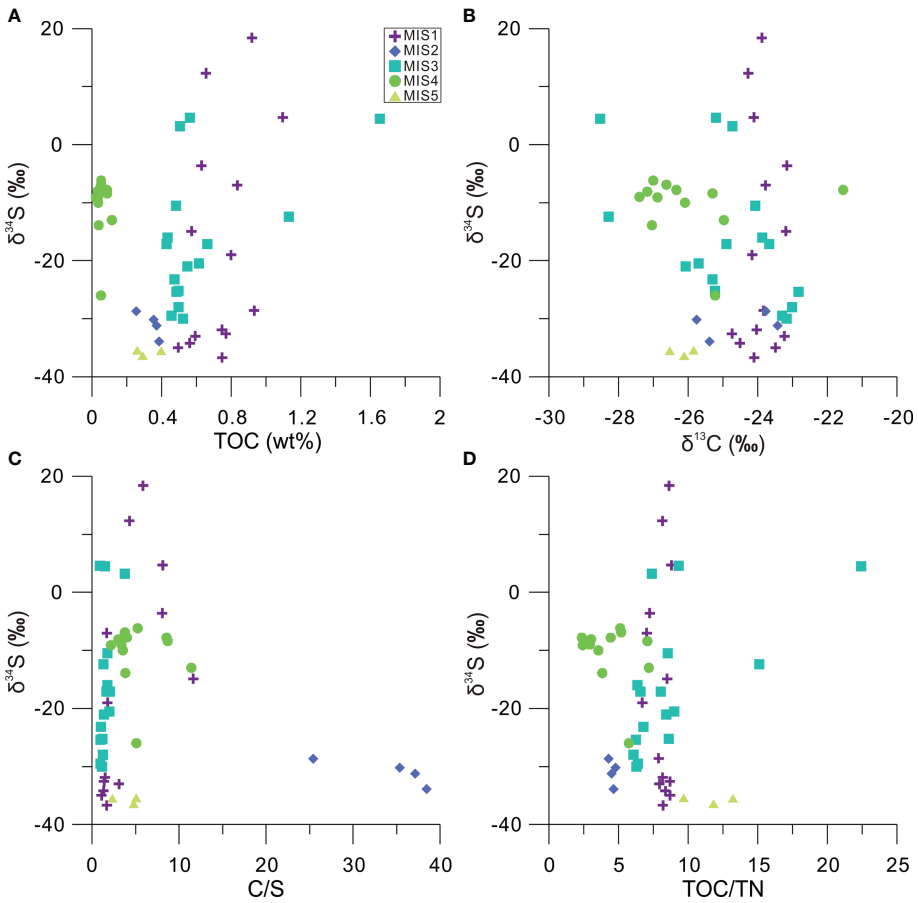

FIGURE 6
The correlation between $\delta^{34}S_{py}$ of pyrite sulfur and TOC content **(A)**, $\delta^{13}C$ of TOC **(B)**, C/S ratio **(C)**, and TOC/TN ratio **(D)**.

organic carbon is also observed at 27 mbsf revealed by TOC/TN ratio and $\delta^{13}C$, where the isotopic composition of pyrite sulfur maintains a high value. We propose that the heavy sulfur isotope is related to the depositional event occurring at 27~34 mbsf of core QK11. And relevant factors, such as the availability and reactivity of organic carbon and sedimentation rates, are worth analyzing.

During the depositional event, the abrupt increased TOC/TN ratios and decreased $\delta^{13}C$ values indicate that the organic carbon is mainly a terrigenous source, which is refractory and not conducive to being utilized by sulfate-reducing bacteria (Meyers, 1997; Blair and Aller, 2012). However, the peak values of TOC and CRS appear together, and the influence of TOC content on the sulfur isotopic composition of pyrite should be evaluated. It is suggested that a high sulfate reduction rate can significantly reduce the sulfur isotopic fractionation of OSR, while high organic carbon content can increase the sulfate reduction rate, which may lead to the positive $\delta^{34}S_{py}$ value (Lin et al., 2002; Leavitt et al., 2013). However, the poor correlation between TOC content and $\delta^{34}S_{py}$ in MIS3 stage sediments shows that high organic carbon content is not responsible for the positive sulfur isotopic signature of pyrite. We speculate that the high sedimentation rates associated with depositional events may be the crucial factor. High sedimentation rate would decrease the connectivity between the porewater sulfate reservoir and the overlying water column to form a relative "closed" diagenetic system (Pasquier et al., 2017; Liu et al., 2019). In this case, local porewater sulfate reservoir becomes enriched in ^{34}S as the sulfate reduction process continues, which leads to produced sulfide and pyrites formed later becoming enriched in ^{34}S. The preponderance of terrigenous materials also implies a great availability of reactive iron in sediments, which has important implications for early diagenetic processes. In the Bornholm Basin, the coupling of high reactive iron contents and heavy sulfur isotope was observed (Liu et al., 2021a). It is interpreted that the high sedimentation rates facilitated the burial of reactive iron and hence the subsurface availability of reactive iron for continued and progressively more ^{34}S-enriched sediment-hosted pyrite formation.

The MIS1 strata are segmented in geochemical indicators including CRS contents, C/S ratios, and $\delta^{34}S_{py}$ With 8 mbsf as the boundary, the lower part maintains a large amount of CRS which is depleted in ^{34}S with an offset higher than 50‰. The upper member is characterized by low CRS contents, high C/S ratios, and isotopically "heavy" pyrite, due to the unsteady diagenetic environment in the ECS (Ge et al., 2015; Zhu et al., 2016). Under such depositional conditions, reoxidation of porewater hydrogen sulfide to sulfate can potentially lead to a minor and even negative value of sulfur isotopic offset between the sedimentary pyrite and original sulfate, and override *in-situ* signals of sulfur fractionation of sulfate reduction and other diagenetic processes (Fry et al., 1988; Fike et al., 2015). And the phenomenon of isotopically "heavy" pyrite also appears on other continental shelves with an unsteady diagenetic environment, such as the Amazon–Guianas mobile mud belt (Aller et al., 2010). In addition, given the abundance of shallow gas (CH_4) buried around Sansha Bay and Xiapu Bay with a depth between 0 and 20 m (Wu et al., 2022), leakage of shallow gas may influence the sulfur isotopic composition of pyrite (Jørgensen et al., 2004; Peketi et al., 2012; Lin et al., 2016; Lin et al., 2017; Miao et al., 2021). However, the coupling of high CRS content and isotopically "heavy" pyrite is not observed in the upper part, indicating that the shallow gas is unlikely to be a significant factor.

Xiapu Bay represented a typical freshwater sedimentary environment during MIS4. The undersupply of porewater sulfate suppressed the sulfate reduction, which resulted in a positive isotopic signature of pyrite sulfur by the sulfate reservoir effect (Gomes and Hurtgen, 2013). Though the sediments of MIS2 interval deposited in a freshwater environment likewise, the sulfur isotopic composition of pyrite is negative, which cannot be explained by the sulfate reservoir effect. The possibilities include the vertical diffusion of hydrogen sulfide in adjacent layers and additional sulfate supplies. The hydrogen sulfide in the MIS1 interval mainly comes from OSR and is depleted in ^{34}S. The hydrogen sulfide diffuses downward and combines with the reactive iron in MIS2 interval, resulting in ^{34}S-depleted pyrite. The diffusion of hydrogen sulfide during OSR would be rather weak in an iron-sufficient environment. Therefore, the CRS contents maintain extremely low values without a sulfidization front in MIS2 interval. In addition, the two adjacent layers of the MIS2 interval were extensively affected by transgressions. After the early diagenesis, the residual porewater sulfate in adjacent layers may migrate vertically to support pyrite formation in the MIS2 interval.

Implications for classical indicators of organic carbon

The effectiveness of C/S ratios has been verified in this study as well as in previous work on the inner shelf of the ECS (Liu et al., 2021c; Liu et al., 2022). Though the C/S ratio can reveal three transgressive layers in the coastal area of southeast China since MIS5, we have to acknowledge that it is also affected by an unsteady diagenetic environment and other sedimentary factors. Therefore, when using C/S ratios to indicate paleosalinity and marine transgression, it is necessary to combine them with other indicators (such as Sr/Ba ratio and TOC/TN ratio) to reduce the risk of making a biased interpretation of depositional evolution (Liu et al., 2022).

The TOC/TN ratio has been widely utilized in the identification of organic carbon sources in estuarine and continental shelf areas (Meyers, 1994; Meyers, 1997; Yu et al., 2011; Zhan et al., 2011). In our study, however, the application of the TOC/TN ratio in terrestrial sedimentary intervals (MIS2 and

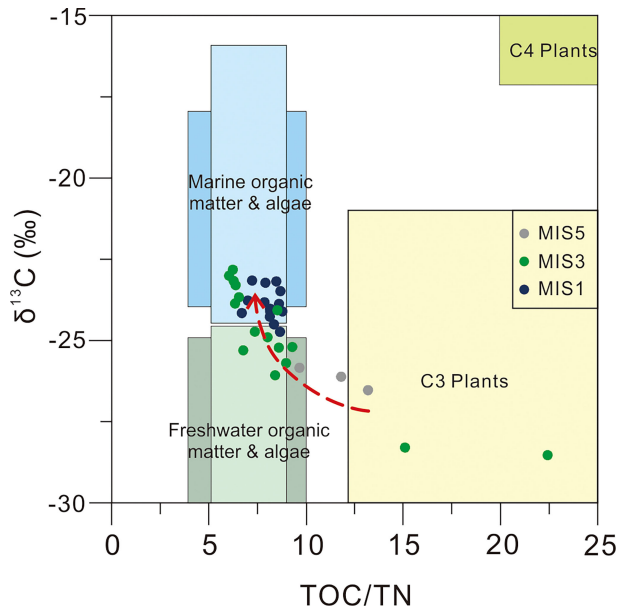

FIGURE 7
Source of organic matter in core QK11 indicated by TOC/TN ratios and $\delta^{13}C$ values. The endmember values refer to Lamb et al. (2006). The red arrow indicates the evolutionary history of organic carbon sources.

MIS4) was severely disturbed due to the low organic carbon content in the sediments and the possible adsorption of inorganic nitrogen by clay minerals (Sampei and Matsumoto, 2001; Hu et al., 2014). But for transgressive strata, the combination of TOC/TN ratio and $\delta^{13}C$ shows that the organic carbon sources in the study area experienced a transition from terrigenous source to marine and terrigenous mixed source to marine source during the three transgressions since MIS5 (Figure 7), which is consistent with the research results that the magnitude of the transgressions gradually increased as revealed by other indicators (C/S ratio, Sr/Ba ratio, etc.). This indicates that TOC/TN ratio and $\delta^{13}C$ can effectively record sedimentary information during transgressions, and should be combined with pyrite-related indicators to indicate depositional evolution.

Conclusions

In this study, we analyzed the depositional evolution history and its influence on the sulfur content and isotope of pyrite in the coastal area of southeast China since MIS5 according to a set of geochemical data from core QK11. The main conclusions are as follows:

1) The positive correlation between TOC and CRS contents in core QK11 indicates that sedimentary pyrite is mainly controlled by TOC in the interglacial transgressive strata. The formation of pyrite during glacial intervals is limited by the supplement of sulfate, inducing extremely low pyrite sulfur contents. Therefore, C/S ratios can effectively identify three transgressions on the Fujian coast since MIS5.

2) Local depositional conditions strongly affect the sulfur isotopic composition of authigenic pyrite in study area during transgressive cycles. The isotopically "heavy" pyrite in core QK11 is attributed to the sulfate reservoir effect, unsteady diagenetic environment, and depositional event.

3) Classical indicators, such as the TOC/TN ratio, are prone to deviation under freshwater sedimentary conditions. It is necessary to combine other geochemical indicators, such as C/S and Sr/Ba ratios, to reconstruct a more reliable history of depositional evolution.

Data availability statement

The original contributions presented in the study are included in the article/Supplementary Material. Further inquiries can be directed to the corresponding authors.

Author contributions

XC: Data curation, Writing- Original draft preparation. XL: Conceptualization, Funding acquisition, Writing- Reviewing and Editing. HW, GZ, ZM, and JY: Writing- Reviewing and Editing. JC: Funding acquisition, Writing- Reviewing and

Editing. All authors contributed to the article and approved the submitted version.

Funding

This work was supported by the National Natural Science Foundation of China (41976053; 41771226) and the Natural Science Foundation of Shandong Province (ZR2021YQ26).

Conflict of interest

The authors declare that the research was conducted in the absence of any commercial or financial relationships that could be construed as a potential conflict of interest.

Publisher's note

Supplementary material

The Supplementary Material for this article can be found online at: https://www.frontiersin.org/articles/10.3389/fmars.2022.1005663/full#supplementary-material

References

Algeo, T. J., Luo, G. M., Song, H. Y., Lyons, T. W., and Canfield, D. E. (2015). Reconstruction of secular variation in seawater sulfate concentrations. *Biogeosciences* 12, 2131–2151. doi: 10.5194/bg-12-2131-2015

Aller, R. C., and Blair, N. E. (1996). Sulfur diagenesis and burial on the Amazon shelf: Major control by physical sedimentation processes. *Geo-Mar. Lett.* 16, 3–10. doi: 10.1007/BF01218830

Aller, R. C., Madrid, V., Chistoserdov, A., Aller, J. Y., and Heilbrun, C. (2010). Unsteady diagenetic processes and sulfur biogeochemistry in tropical deltaic muds: Implications for oceanic isotope cycles and the sedimentary record. *Geochim. Cosmochim. Acta* 74, 4671–4692. doi: 10.1016/j.gca.2010.05.008

Berner, R. A. (1984). Sedimentary pyrite formation: An update. *Geochim. Cosmochim. Acta* 48, 605–615. doi: 10.1016/0016-7037(84)90089-9

Berner, R. A., and Raiswell, R. (1984). C/S method for distinguishing freshwater from marine sedimentary rocks. *Geology* 12, 365–368. doi: 10.1130/0091-7613(1984)12<365:CMFDFF>2.0.CO;2

Bianchi, T. S., Mitra, S., and McKee, B. A. (2002). Sources of terrestrially-derived organic carbon in lower Mississippi river and Louisiana shelf sediments: Implications for differential sedimentation and transport at the coastal margin. *Mar. Chem.* 77, 211–223. doi: 10.1016/S0304-4203(01)00088-3

Blair, N. E., and Aller, R. C. (2012). The fate of terrestrial organic carbon in the marine environment. *Ann. Rev. Mar. Sci.* 4, 401–423. doi: 10.1146/annurev-marine-120709-142717

Borowski, W. S., Rodriguez, N. M., Paull, C. K., and Ussler, W. (2013). Are 34S-enriched authigenic sulfide minerals a proxy for elevated methane flux and gas hydrates in the geologic record? *Mar. Petroleum Geol.* 43, 381–395. doi: 10.1016/j.marpetgeo.2012.12.009

Canfield, D. E. (2001). Biogeochemistry of sulfur isotopes. *Rev. Mineral. Geochem.* 43, 607–636. doi: 10.2138/gsrmg.43.1.607

Canfield, D. E., Raiswell, R., Westrich, J. T., Reaves, C. M., and Berner, R. A. (1986). The use of chromium reduction in the analysis of reduced inorganic sulfur in sediments and shales. *Chem. Geol.* 54, 149–155. doi: 10.1016/0009-2541(86)90078-1

Canfield, D., and Thamdrup, B. (1994). The production of ^{34}S-depleted sulfide during bacterial disproportionation of elemental sulfur. *Science* 266, 1973–1975. doi: 10.1126/science.11540246

Dai, L., Li, S., Yu, J., Wang, J., Peng, B., Wu, B., et al. (2021). Palynological evidence indicates the paleoclimate evolution in southeast China since late marine isotope stage 5. *Quaternary Sci. Rev.* 266, 106964. doi: 10.1016/j.quascirev.2021.106964

Dong, J., Li, A., Liu, X., Wan, S., Feng, X., Lu, J., et al. (2018). Sea-Level oscillations in the East China Sea and their implications for global seawater redistribution during 14.0–10.0 kyr BP. *Palaeogeography Palaeoclimatol. Palaeoecol.* 511, 298–308. doi: 10.1016/j.palaeo.2018.08.015

Dong, J., Li, A., Liu, X., Wan, S., Xu, F., and Shi, X. (2020). Holocene Climate modulates mud supply, transport, and sedimentation on the East China Sea shelf. *J. Geophysical Res.: Earth Surface* 125:e2020JF005731. doi: 10.1029/2020JF005731

Dong, J., Li, A., Lu, Z., Liu, X., Wan, S., Yan, H., et al. (2021). Millennial-scale interaction between the East Asian winter monsoon and El niño-related tropical pacific precipitation in the Holocene. *Palaeogeography Palaeoclimatol. Palaeoecol.* 573:110442. doi: 10.1016/j.palaeo.2021.110442

Fakhraee, M., Hancisse, O., Canfield, D. E., Crowe, S. A., and Katsev, S. (2019). Proterozoic seawater sulfate scarcity and the evolution of ocean–atmosphere chemistry. *Nat. Geosci.* 12, 375–380. doi: 10.1038/s41561-019-0351-5

Fike, D. A., Bradley, A. S., and Rose, C. V. (2015). Rethinking the ancient sulfur cycle. *Annu. Rev. Earth Planetary Sci.* 43, 593–622. doi: 10.1146/annurev-earth-060313-054802

Fry, B., Ruf, W., Gest, H., and Hayes, J. M. (1988). Sulfur isotope effects associated with oxidation of sulfide by O2 in aqueous solution. *Chem. Geol.: Isotope Geosci. Section* 73, 205–210. doi: 10.1016/0168-9622(88)90001-2

Geng, X. (1982). Transgressions and regressions in the eastern China since the late pleistocene epoch. *Acta Oceanol. Sin.* 1, 234–247.

Ge, C., Zhang, W., Dong, C., Dong, Y., Bai, X., Liu, J., et al. (2015). Magnetic mineral diagenesis in the river-dominated inner shelf of the East China Sea, China. *J. Geophysical Res.: Solid Earth* 120, 4720–4733. doi: 10.1002/2015JB011952

Gomes, M. L., and Hurtgen, M. T. (2013). Sulfur isotope systematics of a euxinic, low-sulfate lake: Evaluating the importance of the reservoir effect in modern and ancient oceans. *Geology* 41, 663–666. doi: 10.1130/G34187.1

Habicht, K. S., and Canfield, D. E. (1997). Sulfur isotope fractionation during bacterial sulfate reduction in organic-rich sediments. *Geochim. Cosmochim. Acta* 61, 5351–5361. doi: 10.1016/S0016-7037(97)00311-6

Holmkvist, L., Kamyshny, A., Brüchert, V., Ferdelman, T. G., and Jørgensen, B. B. (2014). Sulfidization of lacustrine glacial clay upon Holocene marine transgression (Arkona basin, Baltic Sea). *Geochim. Cosmochim. Acta* 142, 75–94. doi: 10.1016/j.gca.2014.07.030

Houghton, J., Scarponi, D., Capraro, L., and Fike, D. A. (2021). Impact of sedimentation, climate and sea level on marine sedimentary pyrite sulfur isotopes: Insights from the Valle di manche section (Lower-middle pleistocene, southern Italy). *Palaeogeography Palaeoclimatol. Palaeoecol.* 585, 110730. doi: 10.1016/j.palaeo.2021.110730

Huang, K.-M., and Lin, A. (1995). The carbon-sulfide-iron relationship and sulfate reduction rate in the East China Sea continental shelf sediments. *Geochem. J.* 29, 301–315. doi: 10.2343/geochemj.29.301

Hu, B., Li, J., Zhao, J., Wei, H., Yin, X., Li, G., et al. (2014). Late Holocene elemental and isotopic carbon and nitrogen records from the East China Sea inner shelf: Implications for monsoon and upwelling. *Mar. Chem.* 162, 60–70. doi: 10.1016/j.marchem.2014.03.008

Jørgensen, B. B. (1982). Mineralization of organic matter in the sea bed–the role of sulphate reduction. *Nature* 296, 643–645. doi: 10.1038/296643a0

Jørgensen, B. B., Böttcher, M. E., Lüschen, H., Neretin, L. N., and Volkov, I. I. (2004). Anaerobic methane oxidation and a deep H_2S sink generate isotopically heavy sulfides in black Sea sediments. *Geochim. Cosmochim. Acta* 68, 2095–2118. doi: 10.1016/j.gca.2003.07.017

Kao, S.-J., Hsu, S.-C., Horng, C.-S., and Liu, K.-K. (2004). Carbon-sulfur-iron relationships in the rapidly accumulating marine sediments off southwestern Taiwan. *Geochem. Soc. Special Publ.* 9, 441–457. doi: 10.1016/S1873-9881(04)80031-2

Lamb, A. L., Wilson, G. P., and Leng, M. J. (2006). A review of coastal palaeoclimate and relative sea-level reconstructions using δ13C and C/N ratios in organic material. *Earth-Sci. Rev.* 75, 29–57. doi: 10.1016/j.earscirev.2005.10.003

Lang, X., Tang, W., Ma, H., and Shen, B. (2020). Local environmental variation obscures the interpretation of pyrite sulfur isotope records. *Earth Planetary Sci. Lett.* 533, 116056. doi: 10.1016/j.epsl.2019.116056

Leavitt, W. D., Halevy, I., Bradley, A. S., and Johnston, D. T. (2013). Influence of sulfate reduction rates on the phanerozoic sulfur isotope record. *Proc. Natl. Acad. Sci.* 110, 11244–11249. doi: 10.1073/pnas.1218874110

Lin, J., and Dai, L. (2012). Quaternary marine transgressions in eastern China. *J. Palaeogeogr.* 1, 105–125. doi: 10.3724/SP.J.1261.2012.00009

Lin, S., Huang, K.-M., and Chen, S.-K. (2002). Sulfate reduction and iron sulfide mineral formation in the southern East China Sea continental slope sediment. *Deep Sea Res. Part I* 49, 1837–1852. doi: 10.1016/S0967-0637(02)00092-4

Lin, Z., Sun, X., Lu, Y., Strauss, H., Xu, L., Gong, J., et al. (2017). The enrichment of heavy iron isotopes in authigenic pyrite as a possible indicator of sulfate-driven anaerobic oxidation of methane: Insights from the south China Sea. *Chem. Geol.* 449, 15–29. doi: 10.1016/j.chemgeo.2016.11.032

Lin, Z., Sun, X., Lu, Y., Xu, L., Gong, J., Lu, H., et al. (2016). Stable isotope patterns of coexisting pyrite and gypsum indicating variable methane flow at a seep site of the shenhu area, south China Sea. *J. Asian Earth Sci.* 123, 213–223. doi: 10.1016/j.jseaes.2016.04.007

Lisiecki, L. E., and Raymo, M. E. (2005). A pliocene-pleistocene stack of 57 globally distributed benthic $\delta^{18}O$ records. *Paleoceanography* 20, PA1003. doi: 10.1029/2004PA001071

Liu, J., Antler, G., Pellerin, A., Izon, G., Dohrmann, I., Findlay, A. J., et al. (2021a). Isotopically "heavy" pyrite in marine sediments due to high sedimentation rates and non-steady-state deposition. *Geology* 49, 816–821. doi: 10.1130/G48415.1

Liu, X., Fike, D., Li, A., Dong, J., Xu, F., Zhuang, G., et al. (2019). Pyrite sulfur isotopes constrained by sedimentation rates: Evidence from sediments on the East China Sea inner shelf since the late pleistocene. *Chem. Geol.* 505, 66–75. doi: 10.1016/j.chemgeo.2018.12.014

Liu, X., Li, A., Dong, J., Lu, J., Huang, J., and Wan, S. (2018a). Provenance discrimination of sediments in the zhejiang-fujian mud belt, East China Sea: Implications for the development of the mud depocenter. *J. Asian Earth Sci.* 151, 1–15. doi: 10.1016/j.jseaes.2017.10.017

Liu, X., Li, A., Dong, J., Zhuang, G., Xu, F., and Wan, S. (2018b). Nonevaporative origin for gypsum in mud sediments from the East China Sea shelf. *Mar. Chem.* 205, 90–97. doi: 10.1016/j.marchem.2018.08.009

Liu, X., Li, A., Fike, D. A., Dong, J., Xu, F., Zhuang, G., et al. (2020b). Environmental evolution of the East China Sea inner shelf and its constraints on pyrite sulfur contents and isotopes since the last deglaciation. *Mar. Geol.* 429:106307. doi: 10.1016/j.margeo.2020.106307

Liu, J. P., Li, A. C., Xu, K. H., Velozzi, D. M., Yang, Z. S., Milliman, J. D., et al. (2006). Sedimentary features of the Yangtze river-derived along-shelf clinoform deposit in the East China Sea. *Cont. Shelf Res.* 26, 2141–2156. doi: 10.1016/j.csr.2006.07.013

Liu, J., Pellerin, A., Antler, G., Izon, G., Findlay, A. J., Røy, H., et al. (2021b). Early diagenesis of sulfur in bornholm basin sediments: The role of upward diffusion of isotopically "heavy" sulfide. *Geochim. Cosmochim. Acta* 313, 359–377. doi: 10.1016/j.gca.2021.08.018

Liu, J., Pellerin, A., Antler, G., Kasten, S., Findlay, A. J., Dohrmann, I., et al. (2020a). Early diagenesis of iron and sulfur in bornholm basin sediments: The role of near-surface pyrite formation. *Geochim. Cosmochim. Acta* 284, 43–60. doi: 10.1016/j.gca.2020.06.003

Liu, J. P., Xu, K. H., Li, A. C., Milliman, J. D., Velozzi, D. M., Xiao, S. B., et al. (2007). Flux and fate of Yangtze river sediment delivered to the East China Sea. *Geomorphology* 85, 208–224. doi: 10.1016/j.geomorph.2006.03.023

Liu, X., Zhang, M., Li, A., Dong, J., Zhang, K., Gu, Y., et al. (2022). Sedimentary pyrites and C/S ratios of mud sediments on the East China Sea inner shelf indicate late pleistocene-Holocene environmental evolution. *Mar. Geol.* 450:106854. doi: 10.1016/j.margeo.2022.106854

Liu, X., Zhang, M., Li, A., Fan, D., Dong, J., Jiao, C., et al. (2021c). Depositional control on carbon and sulfur preservation onshore and offshore the oujiang estuary: Implications for the C/S ratio as a salinity indicator. *Cont. Shelf Res.* 227, 104510. doi: 10.1016/j.csr.2021.104510

Lyons, T. W., and Berner, R. A. (1992). Carbon-sulfur-iron systematics of the uppermost deep-water sediments of the black Sea. *Chem. Geol.* 99, 1–27. doi: 10.1016/0009-2541(92)90028-4

Meyers, P. A. (1994). Preservation of elemental and isotopic source identification of sedimentary organic matter. *Chem. Geol.* 114, 289–302. doi: 10.1016/0009-2541(94)90059-0

Meyers, P. A. (1997). Organic geochemical proxies of paleoceanographic, paleolimnologic, and paleoclimatic processes. *Organic Geochem.* 27, 213–250. doi: 10.1016/S0146-6380(97)00049-1

Miao, X., Feng, X., Liu, X., Li, J., and Wei, J. (2021). Effects of methane seepage activity on the morphology and geochemistry of authigenic pyrite. *Mar. Petroleum Geol.* 133, 105231. doi: 10.1016/j.marpetgeo.2021.105231

Morse, J. W., and Emeis, K. C. (1990). Controls on C/S ratios in hemipelagic upwelling sediments. *Am. J. Sci.* 290, 1117–1135. doi: 10.2475/ajs.290.10.1117

Pasquier, V., Sansjofre, P., Rabineau, M., Revillon, S., Houghton, J., and Fike, D. A. (2017). Pyrite sulfur isotopes reveal glacial-interglacial environmental changes. *Proc. Natl. Acad. Sci.* 114, 5941–5945. doi: 10.1073/pnas.1618245114

Peketi, A., Mazumdar, A., Joshi, R. K., Patil, D. J., Srinivas, P. L., and Dayal, A. M. (2012). Tracing the paleo sulfate-methane transition zones and H2S seepage events in marine sediments: An application of c-S-Mo systematics. *Geochem. Geophys. Geosystems* 13:Q1007. doi: 10.1029/2012GC004288

Raiswell, R., and Canfield, D. E. (2012). The iron biogeochemical cycle past and present. *Geochem. Perspect.* 1, 1–220. doi: 10.7185/geochempersp.1.1

Rickard, D. (2012). Microbial sulfide oxidation in sediments *Developments in Sedimentology*. 65, 353–372. doi: 10.1016/B978-0-444-52989-3.00009-X

Sampei, Y., and Matsumoto, E. (2001). C/N ratios in a sediment core from nakaumi lagoon, southwest Japan: Usefulness as an organic source indicator. *Geochem. J.* 35, 189–205. doi: 10.2343/geochemj.35.189

Sampei, Y., Matsumoto, E., Kamei, T., and Tokuoka, T. (1997). Sulfur and organic carbon relationship in sediments from coastal brackish lakes in the shimane peninsula district, southwest Japan. *Geochem. J.* 31, 245–262. doi: 10.2343/geochemj.31.245

Shawar, L., Halevy, I., Said-Ahmad, W., Feinstein, S., Boyko, V., Kamyshny, A., et al. (2018). Dynamics of pyrite formation and organic matter sulfurization in organic-rich carbonate sediments. *Geochim. Cosmochim. Acta* 241, 219–239. doi: 10.1016/j.gca.2018.08.048

Sim, M. S., Bosak, T., and Ono, S. (2011). Large Sulfur isotope fractionation does not require disproportionation. *Science* 333, 74–77. doi: 10.1126/science.1205103

Sun, D.-D., Liu, P., Zhang, J., Yu, J.-J., Yue, W., Wang, J.-L., et al. (2022). Identification and significance of the late pleistocene transgressive strata in the bays if northern fujian province based on geochemical element indicators of sediments. *J. Palaeogeogr.* 24, 139–151. doi: 10.7605/gdlxb.2022.01.011

Tostevin, R., Turchyn, A. V., Farquhar, J., Johnston, D. T., Eldridge, D. L., Bishop, J. K. B., et al. (2014). Multiple sulfur isotope constraints on the modern sulfur cycle. *Earth Planetary Sci. Lett.* 396, 14–21. doi: 10.1016/j.epsl.2014.03.057

Waelbroeck, C., Labeyrie, L., Michel, E., Duplessy, J. C., McManus, J. F., Lambeck, K., et al. (2002). Sea-Level and deep water temperature changes derived from benthic foraminifera isotopic records. *Quaternary Sci. Rev.* 21, 295–305. doi: 10.1016/S0277-3791(01)00101-9

Wang, J., Lin, F., Peng, B., Liu, P., Zhang, C., and Jinxiu, L. (2022). Temporal and spatial characteristics of quaternary stratigraphy in ningde area, fujian province and its indication of sea level changes. *Geol. China*. Available at: http://kns.cnki.net/kcms/detail/11.1167.P.20220314.20221914.20220008.html

Wang, Z., Zhang, J., Mei, X., Chen, X., Zhao, L., Zhang, Y., et al. (2020). The stratigraphy and depositional environments of china's sea shelves since MIS5 (74-128) ka. *Geol. China* 47, 1370–1394. doi: 10.12029/gc20200506

Wei, W., and Algeo, T. J. (2020). Elemental proxies for paleosalinity analysis of ancient shales and mudrocks. *Geochim. Cosmochim. Acta* 287, 341–366. doi: 10.1016/j.gca.2019.06.034

Wei, G.-Y., Chen, T., Poulton, S. W., Lin, Y.-B., He, T., Shi, X., et al. (2021). A chemical weathering control on the delivery of particulate iron to the continental shelf. *Geochim. Cosmochim. Acta* 308, 204–216. doi: 10.1016/j.gca.2021.05.058

Westrich, J. T., and Berner, R. A. (1984). The role of sedimentary organic matter in bacterial sulfate reduction: The G model tested. *Limnol. Oceanogr.* 29, 236–249. doi: 10.4319/lo.1984.29.2.0236

Wu, B., Lin, F., Zhang, Y., Bo, P., and Wang, J. (2022). Distribution characteristics and genesis analysis of submarine shallow gas in ningde coastal area, fujian province. *East China Geol.* 43, 87–93. doi: 10.16788/j.hddz.32-1865/P.2022.01.009

Yu, J., Peng, B., Lan, Y., Bin, W., Jilong, W., Dalin, D., et al. (2021). Palynological record revealed anthropogenic deforestation, Sea level and climate changes since marine isotope stage 5a in the northeastern coast of fujian province. *Earth Sci.* 46, 281–292. doi: doi: 10.3799/dqkx.2019.264

Yu, F., Zong, Y., Lloyd, J. M., Leng, M. J., Switzer, A. D., Yim, W. W. S., et al. (2011). Mid-Holocene variability of the East Asian monsoon based on bulk organic δ13C and C/N records from the pearl river estuary, southern China. *Holocene* 22, 705–715. doi: 10.1177/0959683611417740

Zhang, K., Li, A., Huang, P., Lu, J., Liu, X., and Zhang, J. (2019). Sedimentary responses to the cross-shelf transport of terrigenous material on the East China Sea continental shelf. *Sedimentary Geol.* 384, 50–59. doi: 10.1016/j.sedgeo.2019.03.006

Zhang, K., Li, A., Liu, X., Chen, M.-T., Lu, J., Zhang, J., et al. (2021). Heavy mineral record from the east China sea inner shelf: Implications for provenance and climate changes over the past 1500 years. *Cont. Shelf Res.* 226, 104488. doi: 10.1016/j.csr.2021.104488

Zhan, Q., Wang, Z., Xie, Y., Xie, J., and He, Z. (2011). Assessing C/N and δ13C as indicators of Holocene sea level and freshwater discharge changes in the subaqueous Yangtze delta, China. *Holocene* 22, 697–704. doi: 10.1177/0959683611423685

Zhao, B., Wang, Z., Chen, J., and Chen, Z. (2008). Marine sediment records and relative sea level change during late pleistocene in the changjiang delta area and adjacent continental shelf. *Quaternary Int.* 186, 164–172. doi: 10.1016/j.quaint.2007.08.006

Zhao, B., Yao, P., Bianchi, T. S., Arellano, A. R., Wang, X., Yang, J., et al. (2018). The remineralization of sedimentary organic carbon in different sedimentary regimes of the yellow and East China seas. *Chem. Geol.* 495, 104–117. doi: 10.1016/j.chemgeo.2018.08.012

Zhu, M.-X., Chen, K.-K., Yang, G.-P., Fan, D.-J., and Li, T. (2016). Sulfur and iron diagenesis in temperate unsteady sediments of the East China Sea inner shelf and a comparison with tropical mobile mud belts (MMBs). *J. Geophysical Res.: Biogeosci.* 121, 2811–2828. doi: 10.1002/2016JG003391